Liu *et al. Virology Journal* (2025) 22:19
https://doi.org/10.1186/s12985-025-02636-7

Virology Journal

RESEARCH Open Access

Deciphering the therapeutic effects of Xiyanping injection: insights into pulmonary and gut microbiome modulation, SerpinB2/PAI-2 targeting, and alleviation of influenza a virus-induced lung injury

Tengwen Liu[1†], Shuping Li[2,3†], Xuerui Wang[2,3,4,5†], Mingjiang Liu[6], Yuchen Wang[7], Jie Ying[2], Shuwen Zhang[2], Yan Lin[2,3], Ning Wang[2,3], Yungjing Bai[2,3,4], Lan Xie[8], Tengfei Chen[2,4*], Quansheng Feng[1*] and Xiaolong Xu[2,3,4,5*]

Abstract

Infection with Influenza A virus (IAV) induces severe inflammatory responses and lung injury, contributing significantly to mortality and morbidity rates. Alterations in the microbial composition of the lungs and intestinal tract resulting from infection could influence disease progression and treatment outcomes. Xiyanping (XYP) injection has demonstrated efficacy in clinical treatment across various viral infections. However, its specific effects and mechanisms against IAV remain unclear. In this study, we established an IAV infection mice model, and utilized 16 S rRNA sequencing, RNA sequencing, protein chips, and molecular docking, to investigate the mechanisms of XYP injection on altering pulmonary and gut microbiota, and identifying its target sites. We revealed that XYP injection significantly reduced mortality, weight loss, lung viral titers, and lung pathology in IAV-infected mice. XYP injection down-regulated the activity of malondialdehyde, and the levels of interleukin (IL)-1β, IL-5, IL-6, tumor necrosis factor-α, IL-18, IL-15, granulocyte colony-stimulating factor, IL-9, chemokine (C-C motif) ligand-5, and C-X-C motif chemokine ligand 5, while up-regulated the activities of glutathione peroxidase reactive and superoxide dismutase, and the level of interferon-γ. The diversity of the pulmonary and gut microbiota was altered slightly after XYP injection. The linear discriminant analysis of the gut microbes revealed a higher proportion of potentially beneficial bacteria, including *Akkermansia*, *Parabacteroides goldsteinii*, *Defluviitaleaceae*, *Oscillospirales*, and *Eubacterium_coprostanoligenes_group* characterized the XYP group. Peritoneal macrophage RNA sequencing

†Tengwen Liu, Shuping Li, and Xuerui Wang contributed equally to this work.

*Correspondence:
Tengfei Chen
824053039@qq.com
Quansheng Feng
fengqs118@163.com
Xiaolong Xu
xiaolong_xu3013@126.com

Full list of author information is available at the end of the article

highlighted *Serpinb2* as the most significantly regulated gene by XYP injection, along with consistent changes in multiple downstream Th2 structure genes. KEGG pathway analysis indicated significant modifications in genes associated with influenza A, mitogen-activated protein kinase signaling, nuclear factor kappa-B signaling, and apoptosis following XYP injection. Finally, human protein chips and molecular docking were carried out to confirm the binding of the main component of XYP injection, andrographolide, with SERPINB2/PAI-2 protein. Overall, our study provides valuable insights into the therapeutic potential of XYP injection in treating influenza, highlighting its multifaceted effects on host microbiota and immune responses, and pinpointing SerpinB2/PAI-2 as the target for XYP injection in exerting anti-inflammatory and antiviral therapeutic mechanisms.

Keywords Influenza A virus, Xiyanping, SerpinB2, PAI-2, Andrographolide, Traditional Chinese medicine

Introduction

Influenza, an acute respiratory infection resulting from the Influenza A virus (IAV), presents a significant global health challenge due to its seasonal prevalence and potential for severe illness and mortality [16, 17]. Among seasonal influenza viruses, the H1N1 subtype has been implicated in past pandemics and continues to pose a substantial health burden, particularly when coinciding with outbreaks of other respiratory infections such as COVID-19 [27]. Upon infection, the H1N1 influenza virus manifests early symptoms similar to the common cold, yet its progression can lead to severe complications. Viral replication within host cells weakens the immune response, triggers inflammatory cascades, and disturbs cytokines expression, exacerbating disease severity [22]. Although vaccination remains pivotal in preventing influenza, the antigenic drift of the virus mandates regular updates to vaccines to ensure efficacy [12, 37]. Consequently, there's an imperative to develop adjunctive therapies to complement vaccination efforts.

During IAV infection, the pulmonary and gut microbiota significantly influence host immune responses and disease progression. The pulmonary microbiota inhabits the lower respiratory tract and alveolar spaces. Pathogenic bacteria such as *Streptococcus pneumoniae*, *Haemophilus influenzae*, and *Staphylococcus aureus* directly interact with respiratory mucosal cells or immune cells, thereby impacting the severity of various respiratory infectious diseases, including influenza [2, 25]. Dysbiosis of the gut microbiota also occurs during influenza, characterized by a reduction in beneficial microbes such as *Lactobacillus* and *Bifidobacterium*, and overgrowth of pathogens [32]. This dysbiosis compromises intestinal barrier integrity, leading to systemic inflammation and exacerbating the pathological processes induced by influenza [10]. Importantly, the interactions between the pulmonary and gut microbiota and the host immune system are bidirectional [35]. Respiratory viral infections alter gut microbiota composition, thereby modulating lung immune responses through the gut-lung axis [3]. Modulating the microbiota of the pulmonary or gastrointestinal tract presents an effective strategy for treating influenza infections.

SerpinB2, also known as plasminogen activator inhibitor-2 (PAI-2), serves as a critical modulator of inflammatory responses and oxidative stress [26]. Its expression is notably heightened in activated monocytes and macrophages, particularly during instances of inflammation [31]. Research indicates an augmentation of PAI-2 expression in vitro in response to virus infection, suggesting its implication in the host's immune defense [9, 24]. Studies have also elucidated SerpinB2's intricate involvement in the proliferation and differentiation of monocytes/macrophages, as well as its regulatory function in modulating Th1 and Th2 immunity [43]. During infection, SerpinB2 gene knockout mice (SerpinB2$^{-/-}$) demonstrated a diminished Th2 cytokine response and impaired monocyte recruitment and activation [42]. Additionally, macrophages derived from SerpinB2$^{-/-}$ mice exhibited elevated production of Th1-promoting cytokines and heightened secretion of interferon-γ (IFN-γ), a crucial marker of viral infection, as compared to wild-type cells [30]. This immune imbalance, driven by SerpinB2, may therefore impede the resolution of IAV infection, promoting viral persistence and potentially exacerbating lung tissue damage.

Traditional Chinese Medicine (TCM) has a robust historical precedent in its therapeutic applications for respiratory disorders. Xiyanping (XYP) injection, containing andrographolide sulfonate as its main component derived from *Andrographis paniculata* (Burm.f.) Wall. ex Nees (chuan xin lian), demonstrates broad-spectrum antiviral properties. This patented TCM formula has been employed clinically for treating various viral infections and pneumonia, demonstrating positive adjunctive effects when used in combination with standard therapeutic approaches [20, 38, 41]. Evidence suggests that XYP exhibits heightened antibacterial and anti-inflammatory properties against *Klebsiella pneumoniae* infection in rat models, potentially mediated through inhibition of intracellular pathways such as mitogen-activated protein kinase (MAPK) and nuclear factor kappa-B (NF-κB)(Gu X et al. [13]. However, the effects and mechanisms of XYP in IAV-induced pneumonia remain elusive. In this study, we demonstrated the regulatory effects of XYP injection on inflammatory responses and

oxidative stress in H1N1 virus-infected mice. Furthermore, we observed the modulation of pulmonary and gut microbiota diversity, composition, and functionality following XYP treatment. Through RNA sequencing, we identified *Serpinb2* as a target gene of XYP injection. Additionally, we validated the binding of active XYP ingredients, andrographolide, with PAI-2 (SERPINB2) protein using human protein chips and molecular docking techniques. Our findings offer evidence supporting the use of XYP injection for treating IAV infection, elucidating its regulatory role in both the host immunity and microbiota, and delineating its modulation mechanism targeting SerpinB2/PAI-2.

Materials and methods

Animals

This study was conducted in accordance with the oversight and approval of the Experimental Animal Ethics Committee of Yangzhou University (permit number: 202103-009). Male ICR mice (5 weeks old, weighing 21 ± 2 g) were procured from the Yangzhou University Experimental Animal Center (Production license: SCXK [Jiangsu, China] 2017-0007; Use license: SCXK [Jiangsu, China] 2017-0044). All mice were housed in specific pathogen-free conditions (light/dark cycle: 12 h, temperature: 20 ± 1 ℃, humidity: 30 – 40%) with ad libitum access to food and water. Mice were housed in standard polypropylene cages (size: 25 cm × 15 cm × 12 cm) with sawdust bedding, which was replaced weekly. Prior to experimentation, all mice were acclimatized for 1 day. Experimental procedures were conducted in accordance with the National Institutes of Health Laboratory Research Guidelines.

H1N1 virus infection

The murine-adapted A/Puerto Rico/8/34 (H1N1) influenza strain (PR8 for short) was preserved at -70 ℃ in the Veterinary College of Yangzhou University, China. Zoletil and normal saline (NS) were purchased from Yangzhou University Animal Hospital. As described previously, mice were anesthetized by intraperitoneal injection of 10% Zoletil (50 mg/kg, 0.2 mL), and upon confirmation of sufficient anesthesia depth with mice breathing every 2–3 s, they were intranasally inoculated with 50 μL PR8 virus at the minimum lethal dose (MLD) $_{50}$ [21].

Treatment protocols

The mice were rallocated into: control (CON), model (MOD), XYP at low dosage (LOW), XYP at medium dosage (MIDDLE), XYP at high dosage (HIGH), and dexamethasone (DXMS) groups. Animals were randomly assigned to groups to ensure the fairness and scientific integrity of the experiment. Each mouse was numbered according to its weight and group assignment was made using a computer-generated random sequence.

The CON group was administered intranasal drops of 50 μL NS after anesthesia, and other groups of mice were dripped with 50 μL PR8 at MLD_{50}.

Xiyanping injection (Batch number 240102, 2 mL:50 mg/piece) was made by sulfonation process of andrographolide extracted from *Andrographis paniculata* (Burm.f.) Wall. ex Nees (chuan xin lian), which was provided by Jiangxi Qingfeng Pharmaceutical Co., Ltd. (Ganzhou, China). The CoA were provided in the supplementary materials.

After infection, mice in all experimental groups were treated once a day at a volume of 0.2 mL/d for 7 consecutive days, performed in a BSL-2 laboratory with biosafety Level 2 personal protection. Mice in the MOD group were intraperitoneally injected with NS every day. The LOW, MIDDLE, and HIGH groups were injected intraperitoneally with XYP injection at doses of 7.5, 15, and 30 mg/kg respectively. In the DXMS group, DXMS injection was administered intraperitoneally at 0.1 mg/kg. During the entire experimental period, the mice had free access to water and food. Samples were collected on the 8 days post-infection (dpi) after modeling from the survived mice in each group. Peripheral blood, alveolar lavage fluid, feces, and lung tissues were collected and frozen at -80 ℃. The lung tissue used for pathological examination was fixed in a 4% paraformaldehyde solution. The weight and death status of mice were recorded every day, with their lifespan and survival rate calculated.

Lung histology

Pulmonary lesion scores of lung tissue were performed. Normal lung tissue was scored as 0, with no inflammation, edema, or bleeding visible to the naked eye. Mild lung injury was scored as 1, with mild inflammation, edema symptoms, and no significant bleeding. Lung tissue thickening in individual areas was scored as 2, with obvious inflammation, edema, and bleeding visible. Consolidation of lung tissue with a range of 25-50% was scored as 3, with obvious inflammation, edema, and bleeding visible. Consolidation of lung tissue over 50% was scored as 4, with severe inflammatory reactions, and edema, accompanied by obvious bleeding or necrosis. Lesions such as edema, hemorrhage, and necrosis in the lung tissue were observed and recorded. The alveolar structure, alveolar septa, and infiltration of inflammatory cells and red blood cells of the lung tissue pathological sections were analyzed and recorded.

Lung index

The lungs of mice were surgically excised and immediately weighed. The lung index = (lung weight / body weight) × 100%.

Oxidative stress and inflammatory cytokines measurement

Fifty milligrams of lung tissue were precisely weighed for the preparation of a 10% tissue homogenate. Superoxide dismutase (SOD), glutathione peroxidase (GSH-Px), and malondialdehyde (MDA) oxidative stress assay kits were sourced from Nanjing Jiancheng Bioengineering Institute, China. All assays were performed in accordance with the manufacturer's protocols.

Blood was collected from mouse eyeballs and put into a 1.5 mL centrifuge tube containing heparin anticoagulant, centrifuged at 1000 rpm for 15 min. Upper plasma was collected and stored at -70 ℃ for long-term storage. The plasma samples were sent to China Leitz Biotechnology Co., Ltd. for Luminex multiplex analysis of interferon-γ (IFN-γ), Interleukin-1β (IL-1β), IL-5, IL-6, tumor necrosis factor (TNF) -α, IL-18, IL-15, granulocyte colony-stimulating factor (G-CSF), IL-9, chemokine (C-C motif) ligand-5 (CCL5), C-X-C motif chemokine ligand 5 (CXCL5), and monocyte chemotactic protein 3 (MCP-3) levels.

DNA extraction and high-throughput 16 S rRNA sequencing

Samples of fresh feces and bronchoalveolar lavage fluid (BALF) were promptly frozen in liquid nitrogen for preservation and subsequently stored at -80 °C until total DNA extraction. Amplification of the V3-V4 regions of the 16 S rRNA gene was performed using conventional primer pairs (341 F: CTAYGGGBRGCASCAG, 806R: GGACTACNNGGGTATCTAAT). Amplification quality was assessed, and raw sequences underwent filtration using default parameters in QIIME. Subsequently, sequences were demultiplexed and clustered into operational taxonomic units (OTUs) at the species level (97% similarity threshold). Species annotation was performed using the Mothur method with the SILVA138 SSUrRNA database (threshold set at 0.8–1). α-diversity and β-diversity analyses were conducted using QIIME. To compare community structure differences between groups, MetaStat analysis was employed to identify species with significant between-group differences, or an Anosim analysis was performed using distance matrices between groups. The Anosim result, akin to a p-value, determined whether significant differences existed between groups.

RNA extraction and RNA-sequencing

Total RNA was extracted from peritoneal macrophages using Trizol Reagent (Invitrogen) following the manufacturer's protocol. Illumina HiSeqTM 2000 was utilized for RNA sequencing. DNase I treatment was employed to remove genomic DNA, and RNA was subsequently enriched using oligo (dT) magnetic beads. Scanning was conducted according to the Illumina HiSeqTM 2000 technical manual. Transcript expression levels were quantified using the transcripts per million reads (TPM) method via RNA-Seq by Expectation Maximization (RSEM). Differential expression analysis between samples was performed using DESeq2 or DEGseq. Genes showing|log2FC| ≥1 and a false discovery rate (FDR) of ≤ 0.05 (DESeq2) or FDR of ≤ 0.001 (DEGseq) were considered significantly differentially expressed. Additionally, functional enrichment analysis including Gene Ontology (GO) and Kyoto Encyclopedia of Genes and Genomes (KEGG) pathways was conducted to identify significantly enriched terms and pathways at Bonferroni-corrected p-value ≤ 0.05 compared to the whole-transcriptome background. GO functional enrichment analysis was performed using Goatools, and KEGG pathway analysis was conducted using KOBAS.

Real-time quantitative polymerase chain reaction (real-time PCR)

Two micrograms of total mRNA underwent reverse transcription to cDNA using AMV reverse transcriptase (Promega, Madison, WI). Real-time PCR analysis of gene expression utilized 2x SYBR master mix (Takara, Otsu, Shiga, Japan) on a BIORAD iCycler iQ5 (Bio-Rad, Hercules, CA). Primer sequences are detailed in Table 1, and target gene expression levels were normalized against GAPDH. Duplicate analyses were conducted for each sample.

Table 1 Primer sequences used in real-time PCR

Gene name	Forward primer sequence 5′-3′	Reverse primer sequence 5′-3′
PR8	TAGCATGCATGCTATCGGTACGT	TAGCTATCTAGCTAGCTAGCTA
SerpinB2	TTCCGTGTGAACTCGCATG	TGCGTCCTCAATCTCATCGG
Ccl2	TTTTGAATGTGAAGTTGACCCGTAAATC	GAAGTGCTTGAGGTGGTTGTGG
Il13ra2	GAGGACCCATTCCACCAAGG	GAGTCTGGCCCTGTGTAACC
Tnf:	AGCCCCCAGTCTGTATCCTT	GCTACGACGTGGGCTACAG
Ccl3	CAGCTTATAGGAGATGGAGCTATG	TCACTGACCTGGAACTGAATG
Ccl5	CCAAGTCTTTTCCTCATTCTCG	TTCTCTGGGTTGGCACACACT
Il1a	GCAACTGTTCCTGAACTCAACT	ATCTTTTGGGGTCCGTCAACT
Il1b	AGCTTTCAGGCAGGCAGTATC	TGTCCTGGCTGTAGAGGTGCT
GAPDH	TCCATGACAACTTTGGCATTG	AGTCTTCTGGGTGGCAGTGA

Proteome analysis based on protein chip

The andrographolide standard was fluorescently labeled with biotin, and it was confirmed that the labeled compound still had biological activity. Andrographolide-biotin was further screened for full protein targets using the HuProt™ Human Proteome Chip. After chip scanning, data analysis was performed to obtain raw data and processed standardized data. After completing the protein screening, a statistical table of detected sites that met the threshold and a statistical table of detected proteins whose repeat sites met the threshold was obtained. After obtaining the component comparison results, a list of significantly specifically detected proteins were obtained.

Molecular docking

The X-ray crystal structure of PAI2 (PDB: 1BY7) was obtained from the Protein Data Bank. The protonation state of all compounds was set at pH 7.4, and 3D structures were generated using Open Babel. AutoDock Tools (ADT3) were utilized to prepare and parameterize both the receptor protein and ligands. Docking grid files were generated using AutoGrid within the sitemap, and AutoDock Vina (1.2.0) performed the docking simulations.

Statistical analysis

Data analysis was conducted using SPSS 25.0 statistical software, and graphs were created with GraphPad Prism 8.0 software. Differences between two groups were assessed using the Student's unpaired-sample *t*-test, while multiple comparisons were evaluated using one-way analysis of variance followed by Dunnett's post hoc test. A p-value < 0.05 was considered statistically significant. All data are presented as mean ± SEM.

Results

XYP injection reduced the mortality, weight loss, and virus titer after IAV infection

As depicted in Fig. 1A, compared to the CON group, mice mortality was notably elevated in the MOD group (9-day mortality MOD vs. CON: 40% vs. 0%). Following MOD induction, administration of XYP injection at low, medium, and high doses substantially decreased mouse mortality (9-day mortality: LOW vs. MOD 13.33% vs. 40%; MIDDLE vs. MOD 20% vs. 40%; HIGH vs. MOD 13.33% vs. 40%). Dexamethasone administration decreased the mortality rate among infected mice compared to the MOD group (9-day mortality DXMS vs. MOD 20% vs. 40%).

To further substantiate the therapeutic efficacy of XYP injection against influenza pneumonia, we assessed changes in body weight and viral load in mice across experimental groups. As depicted in Fig. 1B, mice in the CON group exhibited gradual weight gain from day 0 through 8 dpi. In contrast, mice in the MOD group experienced a decline in weight starting from 3 dpi. Administration of medium and high doses of XYP injection significantly ameliorated this weight loss compared to the MOD group, whereas the low dose did not show a significant effect. Dexamethasone treatment did not mitigate weight loss following IAV infection. Figure 1C demonstrates that pulmonary viral load, quantified as RP8 mRNA expression, was markedly elevated in the MOD group compared to the CON group by 8 dpi. Viral load was significantly reduced following administration of low, medium, and high doses of XYP injection compared to the MOD group. While dexamethasone administration did reduce viral load, its efficacy was inferior to that observed with XYP injection.

XYP injection alleviated lung damage of IAV-infected mice

We further investigated the impact of XYP injection on lung pathology following IAV infection. The overall morphology and histopathological analysis of lung tissues from mice in each experimental group are illustrated in Fig. 1D and E. Obvious edema, hemorrhage, and necrosis were seen in the lung tissues of mice in the MOD group. The XYP groups and DXMS groups alleviated the degrees of edema and hemorrhage compared to the MOD group. The lung tissues of the mice in the MOD group lost the complete alveolar structure, of which the alveolar intervals were thickened and the tissue was severely infiltrated by inflammatory cells and red blood cells. Compared with the MOD group, the lung tissues of mice in the three XYP groups still had intact alveolar structure, of which the alveolar intervals were slightly thickened and the infiltration of red blood cells in the tissue was significantly reduced. The infiltration of red blood cells in the lung tissue of mice in the DXMS group was obvious, and the alveolar intervals were thickened.

The changes in lung index paralleled the observations of general morphology (Fig. 1F). Significantly higher lung indices were noted in the MOD group compared to the CON group. Administration of varying doses of XYP injection or dexamethasone effectively reduced the lung indices associated with the infection.

XYP injection regulated the oxidative stress and inflammatory cytokine secretion of IAV-infected mice

To further elucidate the mechanism by which XYP injection reduces mortality in IAV-infected mice, we examined changes in oxidative stress and secretion of inflammatory cytokines at 8 dpi. As shown in Fig. 2A and B, the GSH-Px and SOD activities of lung tissue in the MOD group were significantly lower than that in the CON group. Different doses of XYP injection significantly up-regulated the GSH-Px activity compared to the MOD groups. Low and medium dose of XYP injection

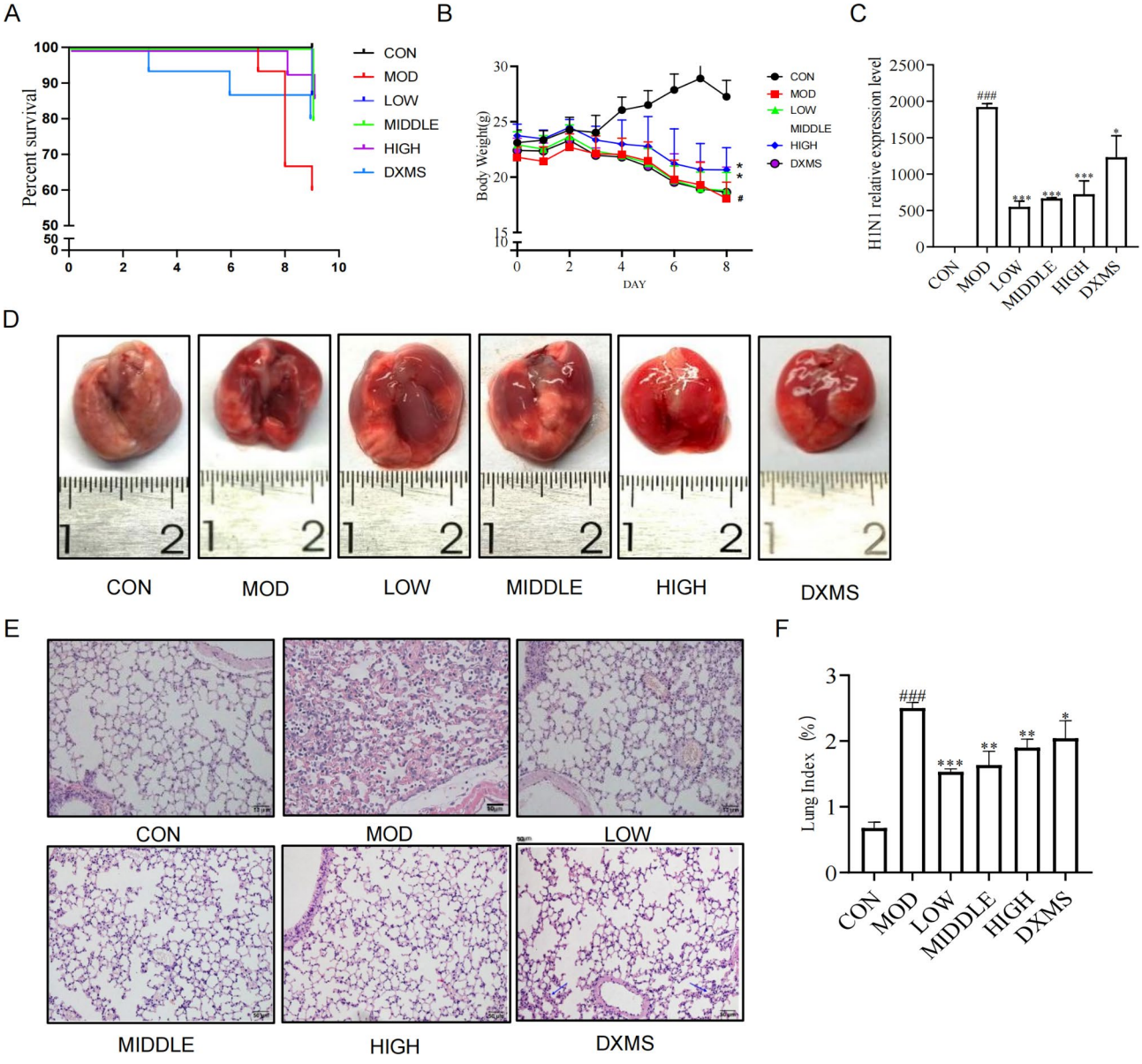

Fig. 1 XYP injection reduced the mortality, weight loss and virus titer after IAV infection. ICR mice were infected with 50 μL of influenza A/Puerto Rico/8/1934 H1N1 (PR8) virus at MLD_{50}, and then receiving intraperitoneal injections of XYP at doses of 7.5 (LOW), 15 (MIDDLE), and 30 mg/kg (HIGH), or dexamethasone (0.1 mg/kg, intraperitoneally) (DXMS) daily for seven consecutive days. Control group mice (CON) were not infected with the virus and received daily intraperitoneal injections of normal saline (0.2 ml) for the same duration. (**A**) Kaplan–Meier survival curves for 9 days. (**B**) Body weight measurements over 8 days. (**C**) Comparison of pulmonary viral loads among groups at 8 days post-infection (dpi). (**D**) General morphology of lung tissues. (**E**) Histopathological assessment of lung sections at 400× magnification (Bar = 50 μm). (**F**) Lung index measurements at 8 dpi for each group. Values represent mean ± SEM of 10 animals per group. Statistical significance is denoted as $^{\#}$ compared with CON, * compared with MOD. $^{*}P < 0.05$, $^{**}P < 0.01$, $^{***}P < 0.001$ for each symbol, respectively

significantly up-regulated the SOD activities compared to the MOD groups. Dexamethasone administration up-regulated the GSH-Px activities, but showed no effects on altering the SOD activities compared to the MOD groups. As depicted in Fig. 2C, the MDA activity in lung tissues of the MOD group was notably elevated compared to the CON group. Administration of XYP injection or dexamethasone significantly attenuated MDA activity compared to the MOD group.

The levels of inflammatory cytokines are shown in Fig. 3. MOD mice exhibited markedly elevated levels of IFN-γ, IL-1β, IL-5, IL-6, TNF-α, IL-18, IL-15, G-CSF, IL-9, CCL-5, CXCL5, and MCP-3 in plasma samples compared to the CON group. High dosages of XYP injection significantly reduced the levels of IL-1β, IL-5, IL-6,

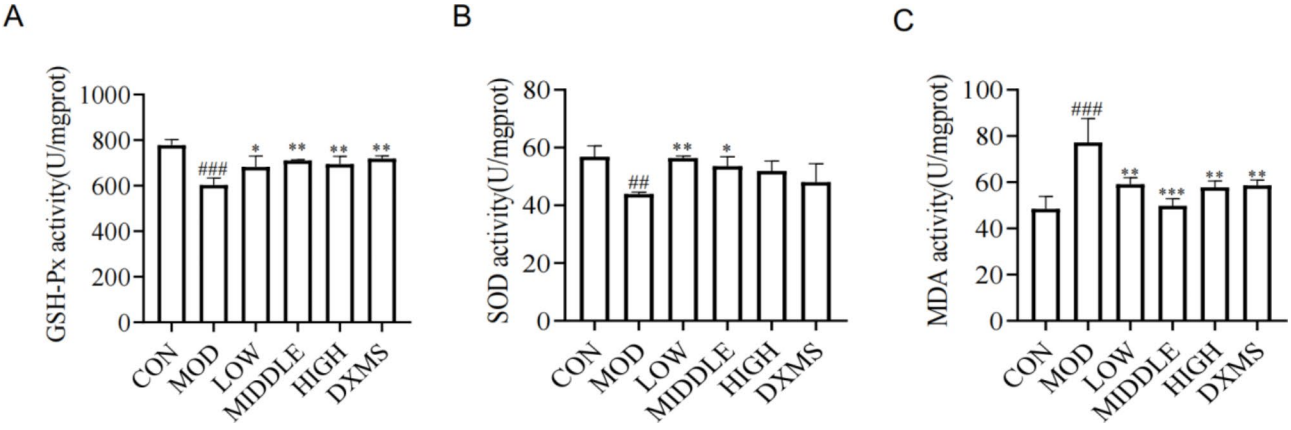

Fig. 2 XYP injection regulated the oxidative stress upon IAV infection. (**A**) Glutathione peroxidase reactive (GSH-Px) activity, (**B**) Superoxide dismutase (SOD) activity, and (**C**) Malondialdehyde (MDA) activity detected from uninfected or infected mice at 8 days post-infection. Values are mean ± SEM of 10 animals per group. #compared with CON, *compared with MOD. *$P<0.05$, **$P<0.01$,***$P<0.001$ of each symbol, respectively

TNF-α, IL-18, IL-15, G-CSF, IL-9, CCL-5, and CXCL5, and significantly up-regulated the secretion of IFN-γ compared to the MOD group. Dexamethasone administration significantly reduced the levels of IL-1β, IL-6, TNF-α, IL-18, IL-15, and G-CSF, and up-regulated the secretion of IFN-γ compared to the MOD group. However, it showed no effects on decreasing the levels of IL-5, IL-9, CCL-5, and CXCL5 in plasma as XYP injection did. Therefore, we demonstrated that XYP injection has anti-inflammatory and antioxidative effects in IAV-infected mice.

XYP injection altered the diversity of pulmonary and gut microbiota

The α-diversity indexes, including Simpson, Shannon, Pielou-e, and the rarefaction curve, were calculated. In the BALF samples, the Simpson, Shannon, and Pielou-e indexes were significantly higher in the MOD, XYP, and DXMS groups compared to the CON group (Fig. 4A-C). The Simpson, Shannon, and Pielou-e indexes showed no difference between the XYP and DXMS groups as compared to the MOD group. The rarefaction curve of alpha diversity showed that the XYP group has the highest species richness and evenness (Fig. 4D). The β-diversity was measured by Nonmetric Multidimensional Scaling (NMDS) and the principal coordinate analysis (PCoA). In the BALF samples, NMDS showed a significant difference among the CON, MOD, XYP, and DXMS groups with a stress = 0.147 (< 0.2, Fig. 4E). PCoA represented distinct microbiome profiles among CON, MOD, XYP, and DXMS groups with pcoa1 of 38.78% and pcoa2 of 17.97% (Fig. 4F).

In the feces samples, the Simpson, Shannon, and Pielou-e indices were significantly lower in the MOD, XYP, and DXMS groups compared to the CON group (Fig. 5A-C). The Simpson, Shannon, and Pielou-e indexes showed no difference between the XYP and DXMS groups as compared to the MOD group. The rarefaction curve of alpha diversity showed that the DXMS group has the lowest species richness and evenness (Fig. 5D). The rarefaction curve showed no significant differences among the CON, MOD, and XYP groups. NMDS showed a significant difference among the CON, MOD, XYP, and DXMS groups with a stress = 0.148 (< 0.2, Fig. 5E). PCoA represented distinct microbiome profiles among the CON, MOD, XYP, and DXMS groups with pcoa1 of 36.96% and pcoa2 of 13.47% (Fig. 5F). Overall, XYP administration slightly altered the structural microbial diversity of the lungs and feces.

XYP injection altered the composition of pulmonary and fecal microbiota

In the BALF samples, Proteobacteria, Firmicutes and Bacteroidota, Desulfobacterota, Fusobacteriota, Myxococcota, and Acidobacteriota were the dominant phyla microbiota (relative abundance >1%) in the CON, MOD, XYP, and DXMS groups (Fig. 6A). In addition, Cyanobacteria and Actinobacteriota were dominant phyla microbiota in the MOD groups. Moreover, the top 3 predominant genera in the CON, XYP, and DXMS groups were *Ralstonia* (89.1%, 63.5%, and 73.2%, respectively), *Delftia* (2.5%, 4.9%, and 3.3%, respectively), and *Pseudomonas* (0.5%, 2.2%, and 2.9%, respectively). The top 3 predominant genera were *Ralstonia* (63.4%), *Klebsiella* (5.6%), and *Delftia* (3.3%) in the MOD group (Fig. 6B).

In the feces samples, Firmicutes, Bacteroidota, Desulfobacterota, Campilobacterota, Patescibacteria, and Deferribacterota were the dominant phyla microbiota (relative abundance >1%) in the CON, MOD, XYP, and DXMS groups (Fig. 6C). In addition, Verrucomicrobiota was a dominant phyla microbiota in the MOD, XYP, and DXMS groups. Actinobacteriota was a dominant phyla microbiota in the MOD group. Moreover, the top 3 predominant genera were *Lactobacillus* (29.7%), *Muribaculaceae*

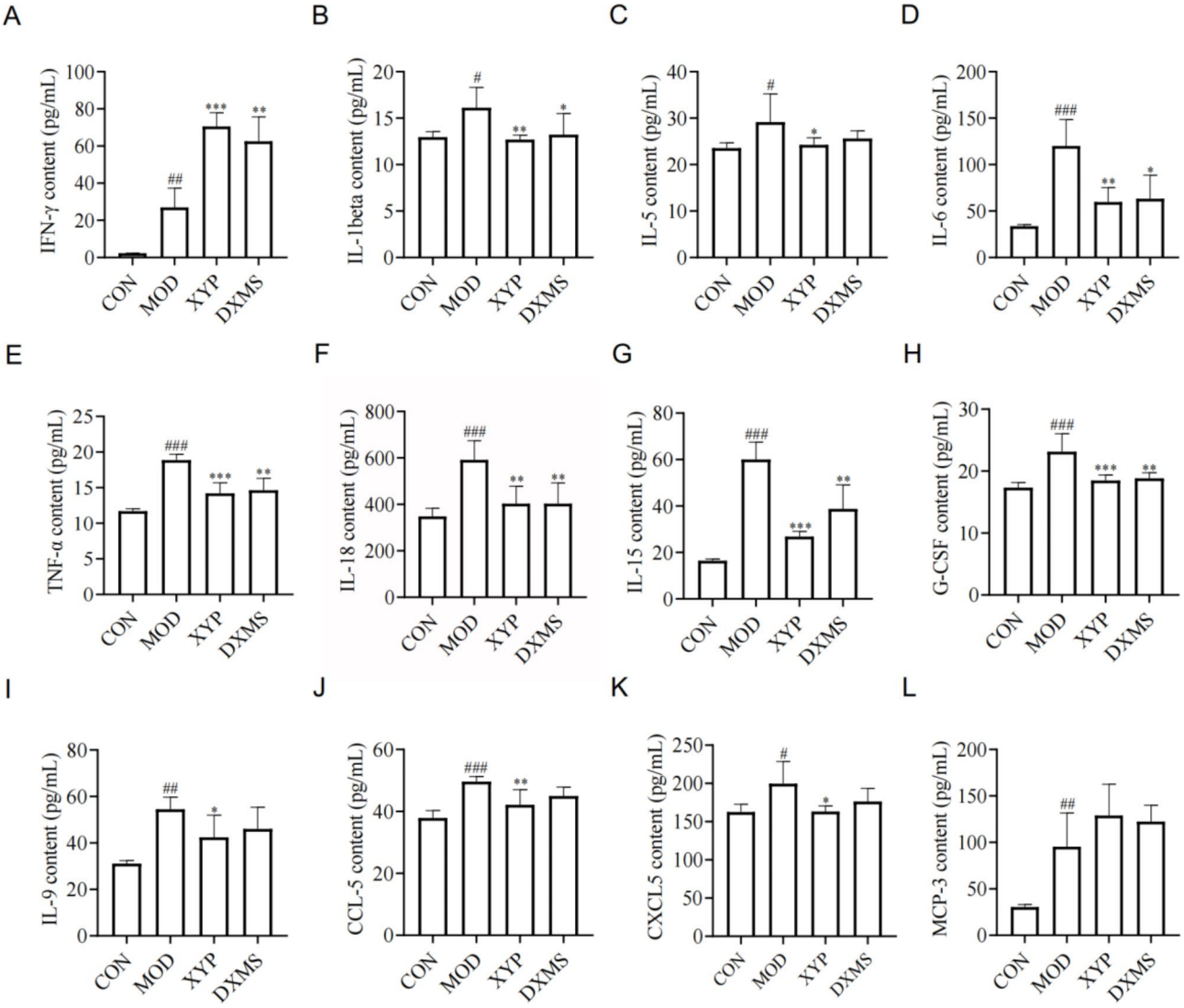

Fig. 3 XYP injection regulated the inflammatory cytokines secretion upon IAV infection. Plasma levels of (**A**) interferon-γ (IFN-γ), (**B**) Interleukin-1β (IL-1β), (**C**) IL-5, (**D**) IL-6, (**E**) tumor necrosis factor-α (TNF-α), (**F**) IL-18, (**G**) IL-15, (**H**) granulocyte colony-stimulating factor (G-CSF), (I) IL-9, (**J**) chemokine (C-C motif) ligand-5 (CCL5), (**K**) C-X-C motif chemokine ligand 5 (CXCL5), and (**L**) monocyte chemotactic protein 3 (MCP-3) detected from uninfected or infected mice at 8 days post-infection. Values are mean ± SEM of 10 animals per group. #compared with CON, *compared with MOD. *$P<0.05$, **$P<0.01$,***$P<0.001$ of each symbol, respectively

(21.9%), and *Alistipes* (4.9%) in the CON group; *Akkermansia* (49.9%), *Lactobacillus* (15.9%), and *Muribaculaceae* (13.1%) in the MOD group; *Akkermansia* (38.3%), *Muribaculaceae* (15.8%), and *Eubacterium_coprostanoligenes_group* (3.6%) in the XYP group; and *Akkermansia* (31.6%), *Muribaculaceae* (18.6%), and *Lactobacillus* (13.4%) in the DXMS group, respectively (Fig. 6D).

Moreover, Linear Discriminant Analysis (LDA) analyses of the differences in microbiota structures from the phylum to the genus level in the BALF and fecal samples were analyzed (Fig. 7A and C). In the BALF samples, a higher proportion of genera *Ralstonia* characterized the CON group, a higher proportion of genera *Rheinheimera* characterized the MOD group, a higher proportion of genera *Phascolarctobacterium* and *Acinetobacter* characterized the XYP group, and a higher proportion of genera *Pseudomonas* characterized the DXMS group (LDA score [log10] > 2) (Fig. 7A). In the feces samples, a higher proportion of genera *Lactobacillus*, *Helicobacter*, and *Allopervotella* characterized the CON group, a higher proportion of genera *Faecalibaculum* characterized the MOD group, a higher proportion of genera *Akkermansia*, *Paludicola*, and *Defluviitaleaceae_UCG_01* characterized the XYP group. No representative bacteria were identified in the DXMS group with LDA score [log10] > 4 (Fig. 7C).

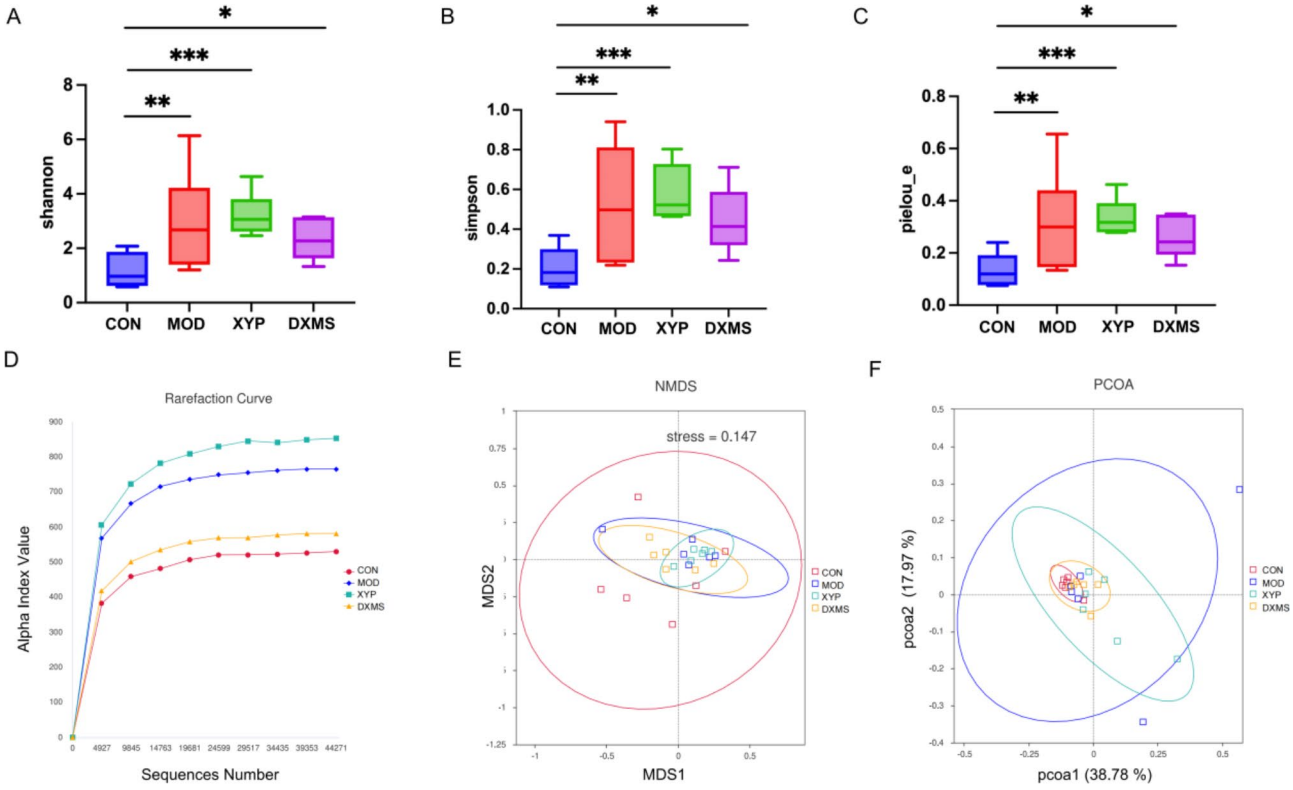

Fig. 4 XYP injection altered the structural diversity of pulmonary microbiota. 16 S rRNA sequencing of the BALF samples in the control (CON), the model (MOD), the XYP (XYP), and dexamethasone (DXMS) groups detected at 8 days post-infection (5 animals per group). α-diversity was evaluated based on the (**A**) shannon, (**B**) simpson, (**C**) pielou_e, and (**D**) rarefaction curve indices of the operational taxonomic unit (OTU) levels. **P* < 0.05, ***P*<0.01,****P*<0.001, respectively. β-diversity was evaluated based on the (**E**) Non-Metric Multi-Dimensional Scaling (NMDS)analysis and (**F**) principal coordinate analysis (PCoA) of the OTU levels

XYP injection changed the potential function of the pulmonary and fecal microbiome

PICRUSt analysis was conducted to project the potential influence of altered pulmonary and fecal microbiomes due to XYP or DXMS administration. Microbiota with a relative abundance exceeding 1% were included in the analysis. In the BALF samples, as shown in Fig. 7B, KEGG pathways on level 2, including metabolism of cofactors and vitamins, energy metabolism, glycan biosynthesis and metabolism, transcription, cellular processes and signaling, enzyme families, immune system, metabolism, genetic information processing, and biosynthesis of other secondary metabolites were lowered in XYP group as compared to MOD group. KEGG pathways including cardiovascular diseases, neurodegenerative diseases, xenobiotics biodegradation and metabolism, endocrine system, signaling molecules and interaction, lipid metabolism, excretory system, metabolism of terpenoids and polyketides, metabolism of other amino acids, and cancers were enriched in XYP group as compared to MOD group.

In the feces samples, as shown in Fig. 7D, KEGG pathways on level 2, including immune system diseases, metabolic diseases, nucleotide metabolism, cancers, signaling molecules and interaction, environmental adaptation, infectious diseases, membrane transport, and enzyme families were lowered in XYP group as compared to MOD group. KEGG pathways including cell motility, cellular processes and signaling, amino acid metabolism, signal transduction, immune system, lipid metabolism, glycan biosynthesis and metabolism, endocrine system, biosynthesis of other secondary metabolites, and transport and catabolism were enriched in the XYP group as compared to MOD group.

Characterization of molecular events elicited by XYP injection based on RNA sequencing and bioinformatic analysis

To further explore the gene targets of XYP injection in regulating inflammation of IAV infection, RNA-sequencing was performed on peritoneal macrophages of MOD and high dose of XYP groups at 8 dpi. ANOVA was employed to identify significantly altered genes (adjusted p-value and false discovery rate < 0.05) among these groups. As shown in Fig. 8A, according to fold changes of MOD vs. XYP group, the top 20 up-regulated genes

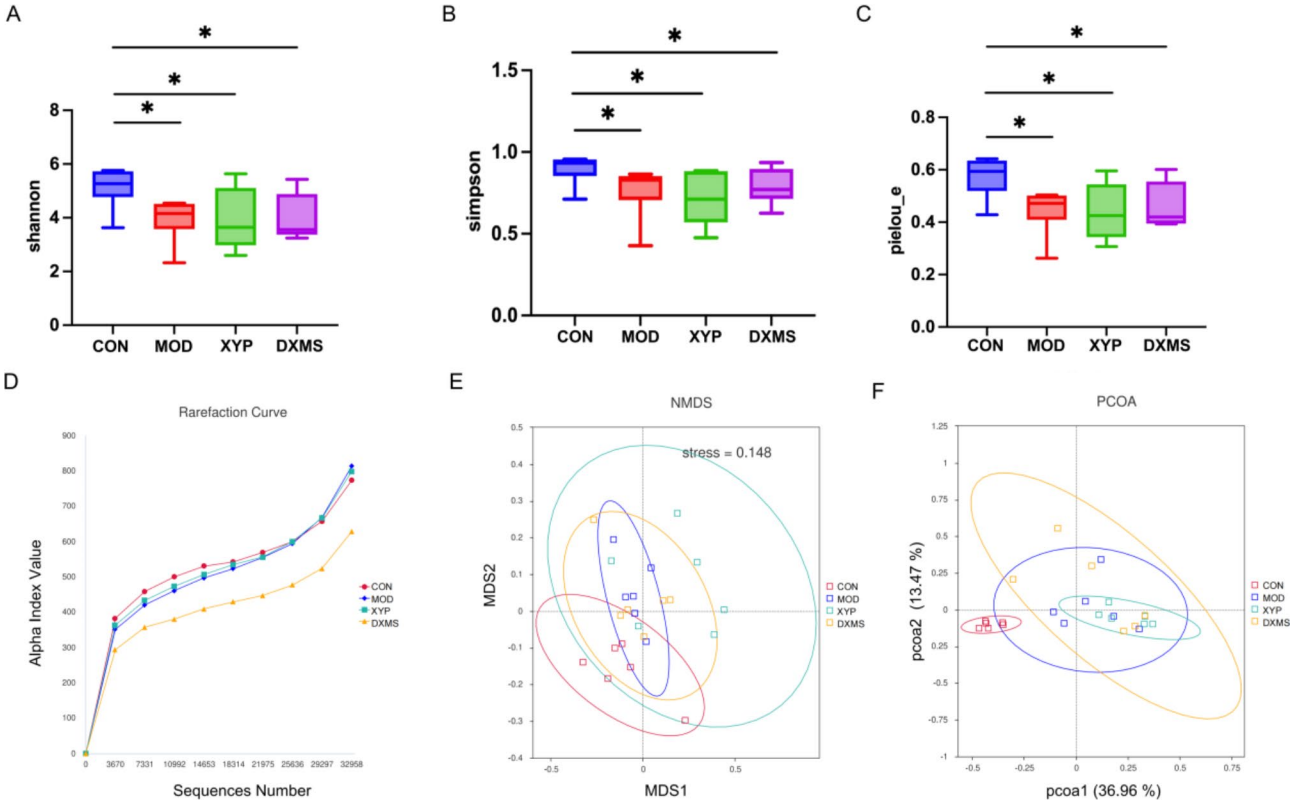

Fig. 5 XYP injection altered the structural diversity of fecal microbiota. 16 S rRNA sequencing of the feces samples in the control (CON), the model (MOD), the XYP (XYP), and the dexamethasone (DXMS) groups detected at 8 days post-infection (5 animals per group). α-diversity was evaluated based on the (**A**)shannon, (**B**) simpson, (**C**) pielou_e, and (**D**) rarefaction curve indices of the operational taxonomic unit (OTU) levels. *$P < 0.05$. β-diversity was evaluated based on the (**E**) Non-Metric Multi-Dimensional Scaling (NMDS)analysis and (**F**) principal coordinate analysis (PCoA) of the OTU levels

were *Serpinb2*, *Snord42b*, *Lcn2*, *Rnu5g*, *Csf3*, *Mirlet7d*, *Il1b*, *Il1a*, *Cxcl2*, *Lif*, *Irg1*, *Cish*, *Nos2*, *Mycl1*, *Col5a3*, *Saa3*, *Il4i1*, *Edn1*, *Ccl22*, *Ccrl2*, and *Socs3*, and the top 20 down-regulated genes were *Rassf3*, *Rasa3*, *Aspm*, *Phf17*, *Sesn1*, *Kifc3*, *Fam78a*, *Zdhhc14*, *Rassf2*, *Ranbp3l*, *Rarb*, *Chst10*, *Lpar5*, *Neurl1b*, *Shb*, *Frmd4b*, *Rnf144b*, *Slc16a12*, *Phyhipl*, and *Hist2h3b*.

As depicted in Fig. 8B, XYP injection markedly decreased the expression levels of the Th2 structure genes, including *Serpinb2*, *Ccl22*, *Socs3*, *Areg*, *Mmp9*, *Ptgs2*, *Ccl7*, *Il10*, *Ccl5*, *Ccl3*, *Il13ra2*, *Ccl4*, *Aloxe3*, *Il10ra*, *Dusp1*, *Il18rap*, *Tgfb1*, *Socs1*, *Il18*, *Socs5*, *Spink5*, *Il10rb*, *Cd200r1*, and *Dusp6* as compared to the MOD group. Bioinformatic analysis includes GO and KEGG pathway analysis. XYP injection significantly altered biological processes including cell proliferation, death, immune system process, and viral reproduction (Fig. 8C) as compared to the MOD group. KEGG pathway analysis showed that genes associated with influenza A, MAPK signaling pathway, NF-κB signaling pathway, signal transducer and activator of transcription (STAT) signaling pathway, apoptosis, etc. were significantly altered after XYP injection (Fig. 8D).

XYP injection reduces Th2 structure and viral infection-related genes in macrophages of IAV-infected mice

As indicated by RNA sequencing, genes encoding Th2 inflammation and viral infection potentially played a crucial role in the protective effects induced by XYP injection. These gene profiles were further validated using real-time PCR. The mRNA levels of *Serpinb2*, *Ccl22*, *IL13ra*, *Tnf*, *Ccl3*, *Ccl5*, *IL1a*, and *IL1b* were significantly up-regulated in peritoneal macrophages of the MOD group as compared to the CON group (Fig. 9). A particularly notable observation was that XYP injection significantly down-regulated these Th2 structure and viral infection-related genes as compared to the MOD group (Fig. 9).

SERPINB2/PAI2 serves as the target of XYP injection

As indicated by RNA sequencing that SerpinB2 is the potential gene target of XYP injection, we further determined the potential protein target of andrographolide-biotin using the HuProt™ human proteome chip. More than 500 potential direct-binding target proteins were obtained. Through literature search analysis combined with KEGG/STRING correlation viral pneumonia bioinformatics analysis, SERPINB2 (PAI-2), which is encoded

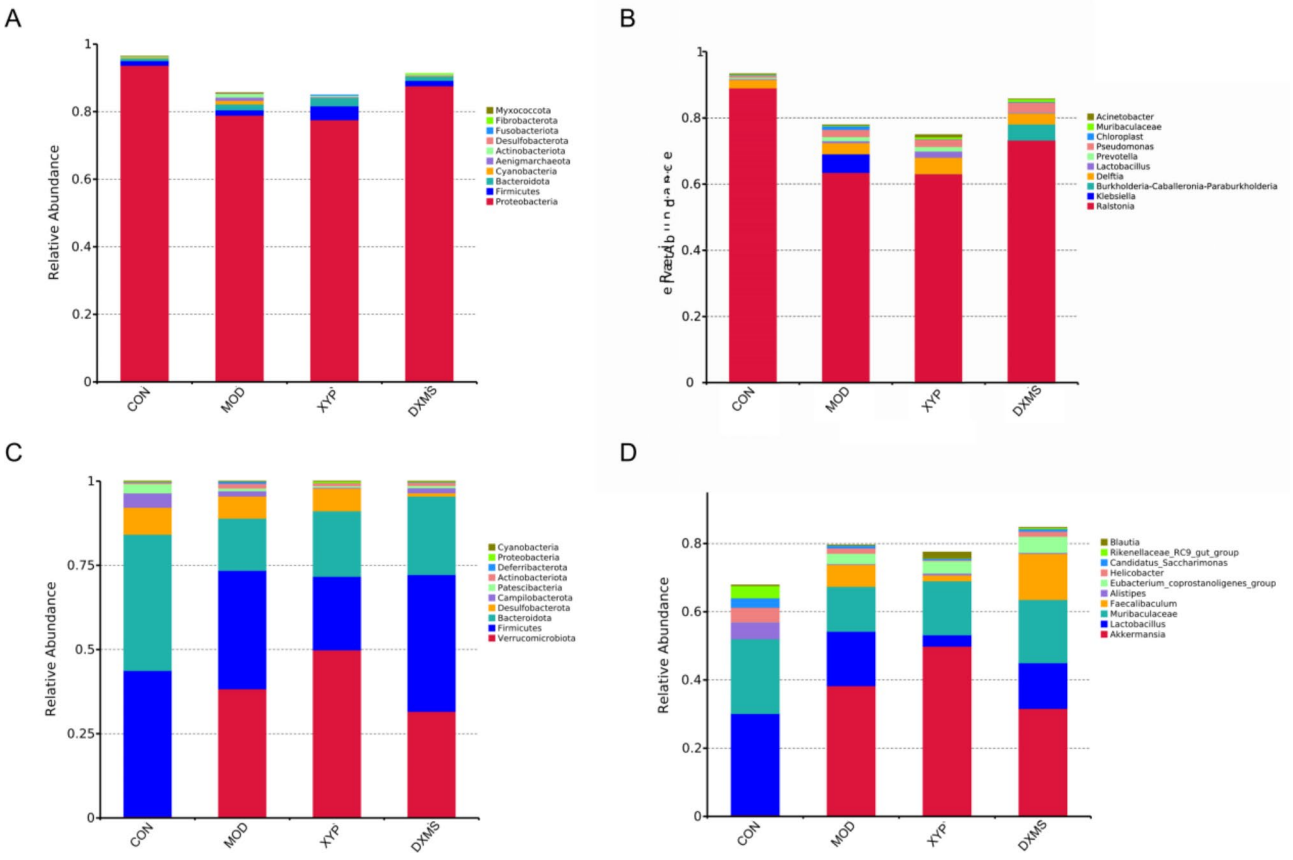

Fig. 6 XYP injection altered the composition of pulmonary and fecal microbiota. 16 S rRNA sequencing of the feces samples in the control (CON), the model (MOD), the XYP (XYP), and the dexamethasone (DXMS) groups detected at 8 days post-infection (5 animals per group). The percentage of community abundance at the phylum (**A**) and genus (**C**) levels of the pulmonary samples, and the percentage of community abundance at the phylum (**B**) and genus (**D**) levels of the fecal samples

by SerpinB2 genes, was identified as the key target protein of andrographolide in exerting its antiviral effect (SNR 13.3, I-mean ratio 15.77) (Fig. 10A). We further analyzed the interactions between PAI-2 protein and ligands. 14-deoxy-11-oxoandrographolide, 14-deoxy-12-methoxyandrographolide, 14-deoxyandrographolide, and andrographolide-19-β-D-glucoside are 4 types of andrographolide derivatives in XYP injection. We analyzed the interaction forces generated by their binding to PAI-2, and made classification criteria according to the interactions. The results showed that receptor proteins and small molecules directly formed multiple sets of interaction forces, which indicated that those derivatives had considerable binding abilities to PAI-2. The binding energy of 14-deoxy-11-oxoandrographolide's protein-small molecule complex was −6.8 kcal/mol (Fig. 10B), and that of 14-deoxy-12-methoxyandrographolide's was −5.5 kcal/mol (Fig. 10C), of 14-deoxyandrographolide's was −6.5 kcal/mol (Fig. 10D). The binding energy of andrographolide-19-β-D-glucoside's was −7.3 kcal/mol (Fig. 10E), with the strongest interaction ability and the largest number of binding sites.

Discussion

Excessive lung injury and subsequent pneumonia are the main causes of influenza infection progressing into a severe scenario. The aggravation and mortality are caused by two factors: damage to lung tissue and an excessive inflammatory response. Andrographolide, the primary constituent of XYP Injection, demonstrates broad-spectrum antiviral activity against pathogens including IAV, hepatitis C virus, herpes simplex virus, and Epstein–Barr virus [15]. Andrographolide could exert regulatory effects on multiple stages of viral replication, including viral attachment, replication, and release. A study has demonstrated the high-affinity binding of andrographolide to IAV surface hemagglutinin and neuraminidase, thereby impeding viral attachment to target cells and the release of new viral particles [29]. Additionally, andrographolide disrupts essential viral protein functions; for instance, it can deactivate HCV NS3/4A protease, which is crucial for RNA replication and signal transduction [5]. Recent findings also suggest its potential to bind effectively to the main protease of SARS-CoV-2, hinting at a possible role in inhibiting COVID-19

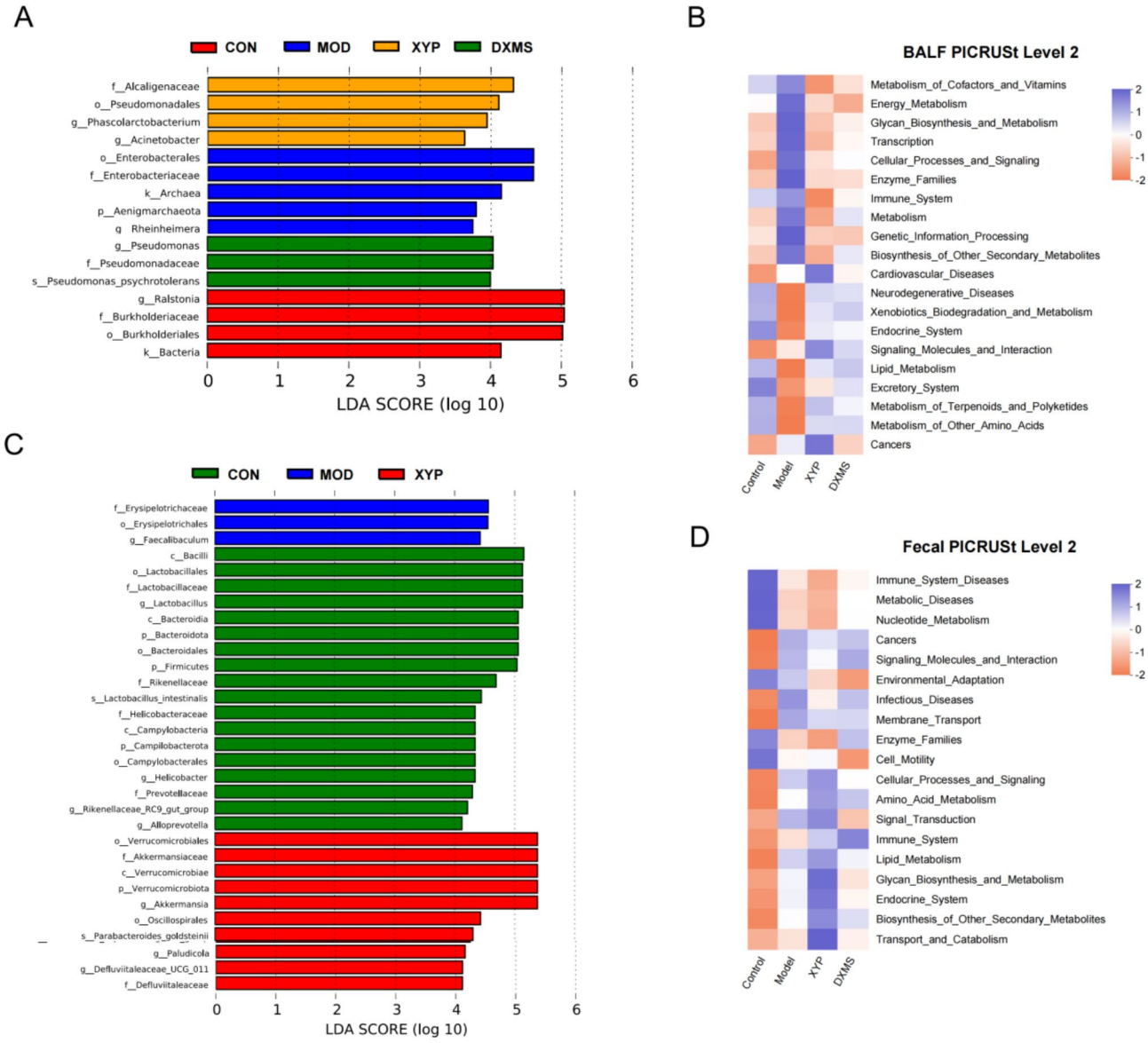

Fig. 7 Linear discriminant analysis (LDA) integrated with effect size (LEfSe) and KEGG pathway using PICRUSt2 software. The differences in pulmonary (**A**) and feces (**C**) bacteria abundance among the control (CON), the model (MOD), the XYP (XYP), and the dexamethasone (DXMS) groups. KEGG pathway enriched in pulmonary (**B**) and feces (**D**) among the 4 groups

replication and spread [1]. In our study, we first evaluated the efficacy of XYP injection in mice infected with the H1N1-influenza virus. We employed three concentration gradients of XYP injection, with dexamethasone used as a positive drug control. The results demonstrated that all three concentrations of XYP injection significantly ameliorated the mortality rate, lung injury, and viral titers in mice infected with the H1N1-influenza virus. Although the medium-dose group showed slightly higher mortality than the high-dose group, no significant difference was found between them. Both medium and high doses significantly alleviated weight loss, with the high dose showing the greatest effect. Therefore, the high dose was chosen for subsequent experiments due to its superior therapeutic efficacy. Compared to the positive control dexamethasone, XYP injection demonstrated a more significant reduction in viral titers and weight loss, suggesting potential advantages, although further studies are required to confirm these findings.

Andrographolide is recognized not only for its antiviral effects but also for its potent anti-inflammatory properties. In both in *vitro* and in *vivo* studies, andrographolide treatment has demonstrated the ability to suppress pro-inflammatory cytokine production through modulation of the Janus kinase (JAK)-STAT signaling pathway and subsequent transcription factors like

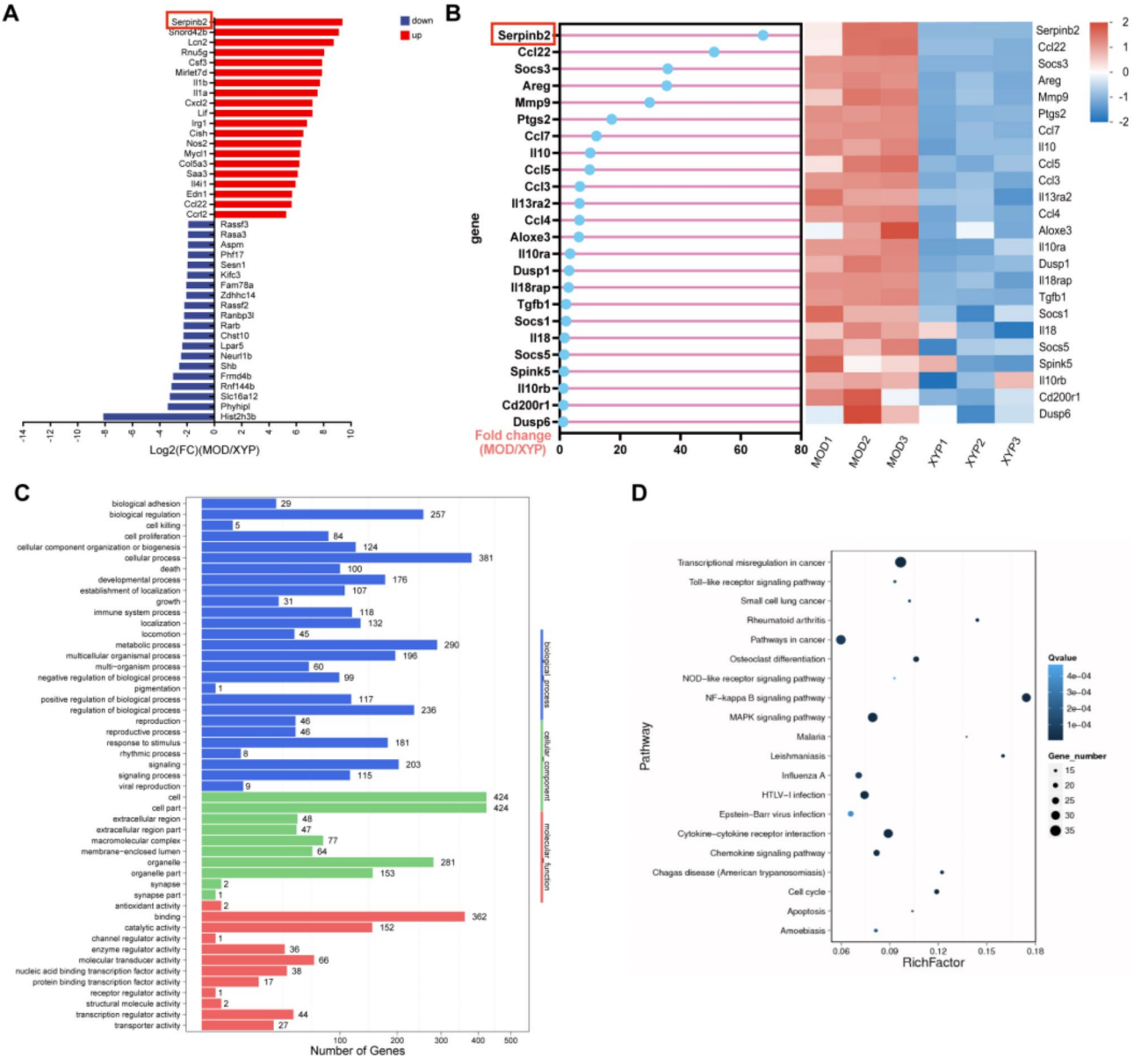

Fig. 8 Characterization of molecular events elicited by XYP injection based on RNA sequencing and bioinformatic analysis. Transcriptional profiling and bioinformatic analysis of peritoneal macrophages in control (CON) and IAV-infected treated with (XYP) or without XYP injection (MOD) at 8 days post-infection ($n=3$ per group). (**A**) Top 20 up- and down-regulated genes according to $\log_2$ fold change in transcriptional profiling. (**B**) Expressions of Th2 structure-related genes in the MOD and XYP groups. (**C**) GO analysis and (**D**) KEGG pathway enrichment analysis of differentially expressed genes. -LgP represents the logarithm of *P* value

NF-κB [8, 11]. It was also reported to reduce virus-induced inflammation by increasing the expression of caspase-1, cleaved caspase-1, cleaved IL-1β, and gasdermin D to inhibit epithelial cell apoptosis and promoting pyroptosis [6]. We observed a significant increase in the activity of GSH-Px and SOD in lung tissues following XYP injection, accompanied by a decrease in MDA levels, as compared to the MOD group, indicating its pronounced antioxidative effects. The results show that XYP injection significantly reduced the levels of several pro-inflammatory cytokines, including IL-1β, IL-5, IL-6, and TNF-α, which are key mediators of the inflammatory response. IL-1β and TNF-α are critical for the activation of inflammatory pathways, inducing fever and immune cell recruitment, while IL-6 is involved in both inflammation and the acute phase response. IL-5, in particular, plays a role in eosinophil recruitment, which is important for modulating the immune response to viral infections. Simultaneously, XYP injection enhanced the secretion of IFN-γ, a key cytokine involved in antiviral defense, which promotes Th1 responses, helping to control viral replication. The functional relationship among these

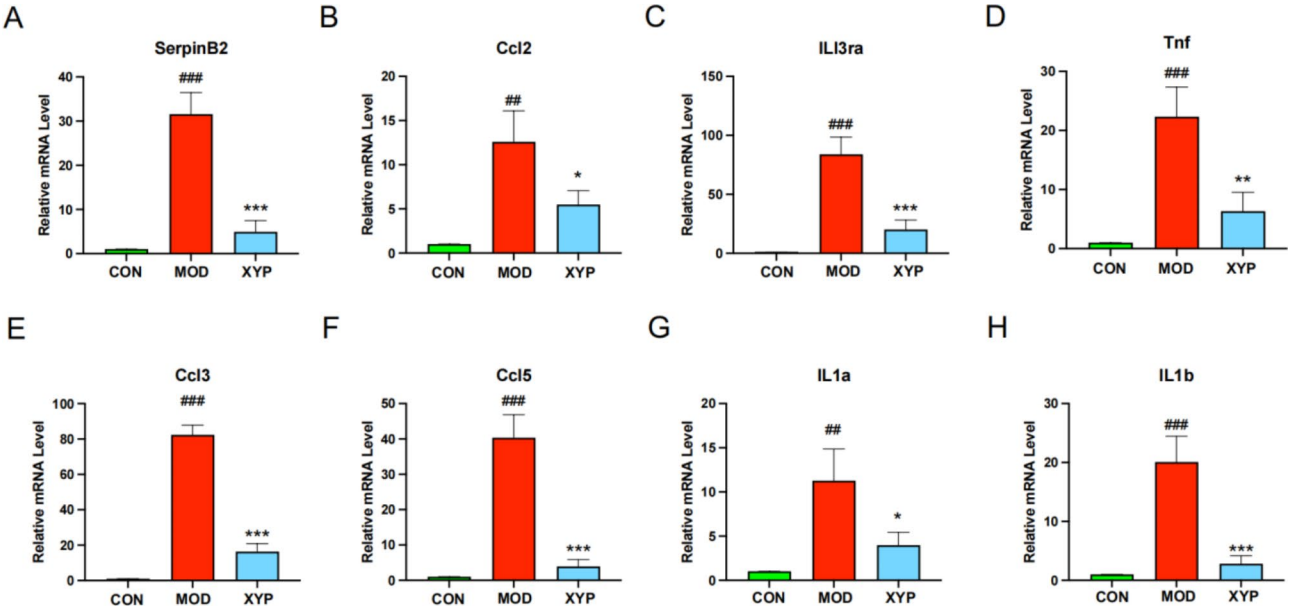

Fig. 9 XYP injection reduces Th2 structure and viral infection-related genes in macrophages of IAV-infected mice. Gene expressions of (**A**) *Serpinb2*, (**B**) *Ccl22*, (**C**) *Il13ra*, (D) *Tnf*, (**E**) *Ccl3*, (**F**) *Ccl5*, (**G**) *Il1a*, and (**H**) *Il1b* were detected by real-time PCR ($n=6$ per group). Values are mean ± SEM. $^{\#}$compared with CON, *compared with MOD. *$P<0.05$, **$P<0.01$,***$P<0.001$ of each symbol, respectively

inflammatory factors was further explored by comparing XYP injection to dexamethasone treatment. While dexamethasone also reduced multiple pro-inflammatory cytokines, it was less effective than XYP in lowering the levels of Th2-related markers, such as IL-5, IL-9, CCL5, and CXCL5. These factors are critical for immune cell recruitment and tissue inflammation, particularly in viral infections. IL-5 and IL-9 are key Th2 cytokines that promote eosinophil recruitment, while CCL5 and CXCL5 are chemokines that facilitate the migration of immune cells, such as T cells and neutrophils, to the site of infection. In line with this trend, our subsequent comparison of macrophage RNA sequencing results between the model group and the XYP injection group revealed that XYP injection downregulated the expression of various Th2-related inflammatory genes. Additionally, KEGG pathway analysis of the RNA sequencing demonstrated that XYP injection exhibited regulatory effects on multiple signaling pathways, including the MAPK signaling pathway, NF-κB signaling pathway, STAT signaling pathway, and apoptosis. These findings further corroborate the beneficial effects of XYP injection on the inflammatory response following IAV infection.

In this study, BALF samples were selected to visualize the microbial population of the lower respiratory tract. Although there were minor differences in the diversity of pulmonary microbiota between the XYP injection or positive drug dexamethasone groups compared to the MOD group, our results revealed significant variations in the composition of dominant bacterial genera among them. We revealed an increased proportion of *Lactobacillus*, a common probiotic, in the XYP group as compared to the MOD group, with no significant alternation in the DXMS group as compared to the MOD group (CON 0.03%, MOD 0.5%, XYP 1.9%, and DXMS 0.2%). *Klebsiella pneumoniae* is a common pathogenic bacterium causing pneumonia [34]. We found that the genus *Klebsiella* was significantly downregulated after treatment with dexamethasone or XYP injection (CON 0%, MOD 0.5%, XYP 0%, and DXMS 0%). In the LDA effect size (LEfSe) analysis, we found that the genus *Phascolarctobacterium* represented the XYP injection group. This genus can produce short-chain fatty acids, including acetate and propionate, which are closely associated with host metabolism and disease states [36]. These results indicated that XYP injection may have potential beneficial regulatory effects on the pulmonary microbiota after IAV infection.

We did not observe significant differences in fecal microbiota alpha diversity between the model group and the XYP group, which may be attributed to the fact that XYP is administered *via* direct intraperitoneal injection rather than orally, which requires digestion and absorption through the intestine. Previous studies have demonstrated that a reduction in the richness of fecal commensal communities may be associated with increased mortality from IAV infection in mice, while probiotic administration has been shown to treat influenza [39]. Our LDA effect size (LEfSe) analysis results suggest that XYP injection significantly increased the abundance of potential beneficial gut microbes, including *Akkermansia*, *Parabacteroides goldsteinii*, *Defluviitaleaceae*, *Oscillospirales* and *Eubacterium_coprostanoligenes_group*. *Akkermansia*

A

Andrographolide-biotin	SNR	Î	I-mean-ratio
SERPINB2 (PAI-2)	15.4	22.34	18.34

B

Receptor: PAI2 (PDB: 1BY7)	Ligand: 42895-57-8	-6.8kcal/mol
Hydrogen bond interaction	ILE114	3.1Å
Electrostatic interaction	\	
hydrophobic interaction	\	

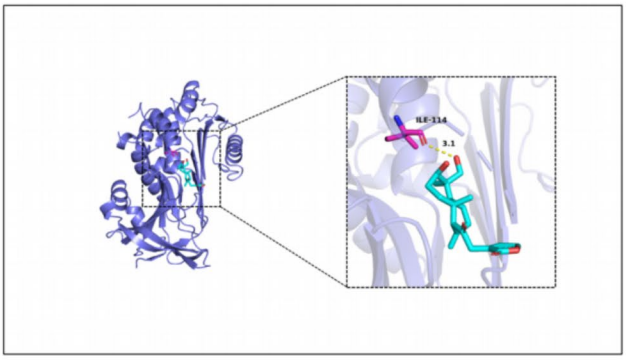

C

Receptor: PAI2 (PDB: 1BY7)	Ligand: 10473975	-5.5kcal/mol
Hydrogen bond interaction	LEU123	3.2Å
	ALA259	3.4Å
	GLY260	3.1Å, 3.2Å
Electrostatic interaction	\	
hydrophobic interaction	\	

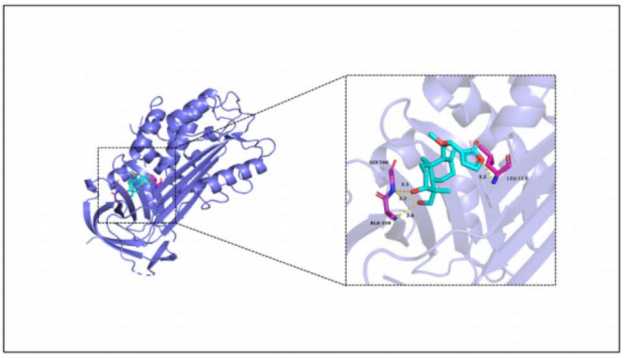

D

Receptor: PAI2 (PDB: 1BY7)	Ligand: 82209-74-3	-6.5kcal/mol
Hydrogen bond interaction	LYS207	2.8Å
	LYS207	3.1Å
	ALA259	3.2Å
Electrostatic interaction	\	
hydrophobic interaction	\	

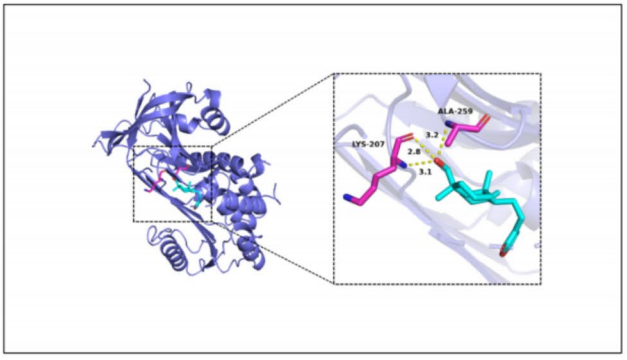

E

Receptor: PAI2 (PDB: 1BY7)	Ligand: 82209-74-3	-7.3kcal/mol
Hydrogen bond interaction	ASP303	3.0Å
	ILE243	2.7Å, 3.4Å
	ALA301	3.2Å, 3.3Å
	LYS299	3.1Å, 2.9Å
	TYR245	3.1Å
Electrostatic interaction	\	
hydrophobic interaction	\	

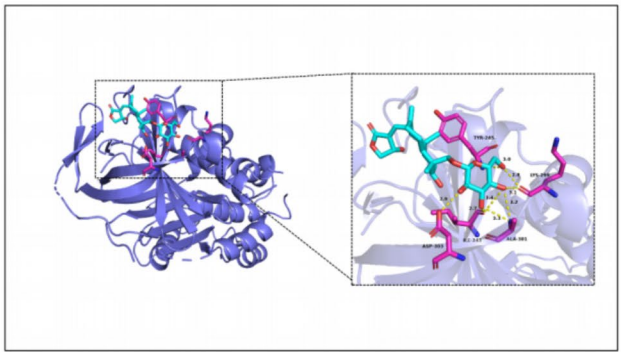

Fig. 10 Binding of andrographolide derivatives and SERPINB2/PAI-2. (**A**) The details of the bonding information of SERPINB2/PAI-2 in the biotin control and the andrographolide-biotin of HuProt™ human proteome chip. The binding evaluation of 4 types of andrographolide derivatives in XYP injection and SERPINB2/PAI-2 is shown in the protein-ligand interaction generated by PyMOL, i.e., (**B**)14-deoxy-11-oxoandrographolide, (**C**) 4-deoxy-12-methoxy-andrographolide, (**D**) 14-deoxyandrographolide, and (**E**) andrographolide-19-β-D-glucoside. The SERPINB2/PAI-2 protein is represented as a slate cartoon model, and the ligand is shown as a cyan stick, and their binding sites are shown as magenta stick structures. Nonpolar hydrogen atoms are omitted. The hydrogen bond, ionic interactions, and hydrophobic interactions are depicted as yellow, magentas, and green dashed lines, respectively

muciniphila contributes to the maintenance of a healthy intestinal barrier, regulating immunity, and limiting inflammation, which is crucial for accelerating recovery post-IAV infection [4]. Additionally, supplementation with *Akkermansia* bacteria or its outer membrane protein Amuc_1100 has been found to alleviate symptoms of enteritis in mice [14]. *Parabacteroides goldsteinii* is an effective inhibitor for preventing intestinal damage caused by bacterium [18]. The intestinal microbial *Defluviitaleaceae* shows potential as a probiotic for influenza prevention [40]. *Eubacterium_coprostanoligenes_group* and *Oscillospirales* are butyric acid-producing bacteria that regulate human metabolism through the decomposition of food scraps and other organic waste into beneficial substances such as butyric acid [19, 33]. Based on the findings described above, we hypothesize that the mechanism of action of XYP injection is related to the alterations in specific gut microbiota. The alterations in gut microbiota may impact pulmonary immune responses and facilitate recovery from influenza via the gut-lung axis. SCFAs, particularly acetate and propionate, produced by gut bacteria such as *Phascolarctobacterium* and *Akkermansia*, are known to enter systemic circulation and influence immune cells in the lungs. These metabolites can reduce lung inflammation and enhance antiviral immunity, suggesting that XYP's effects could be mediated through the gut-lung axis. However, the lack of experiments like fecal microbiota transplantation or antibiotic treatment to deplete the microbiota limits our ability to establish a causal relationship between microbiota changes and the therapeutic effects of XYP.

To further elucidate the mechanism and targets of immune-inflammatory regulation by XYP injection following IAV infection, we utilized RNA sequencing to evaluate the transcriptional alterations in peritoneal macrophages of mice from the MOD and the XYP groups. We found that among the various genes regulated by XYP injection, the alteration in *Serpinb2* was the most significant. SerpinB2, also known as PAI-2, exerts a multifaceted role in viral infections through diverse mechanisms. It modulates immune responses, particularly the balance between Th1 and Th2 immune reactions, which in turn impacts the host's immune status during and after viral infection [31]. Specifically, Serpinb2 has been shown to suppress Th1 cytokines such as IFN-γ, while promoting Th2 cytokines like IL-4, thus shifting the immune response towards a Th2-dominant profile [23, 28]. This shift in the immune microenvironment can promote viral persistence, as the Th2 response tends to support viral survival rather than clearance. In addition to its role in immune modulation, Serpinb2 regulates cell survival and viral replication. By inhibiting apoptosis through suppression of caspase activation, Serpinb2 prolongs the survival of infected cells, providing a favorable environment for viral replication [7]. Consistent with previous studies, our RNA sequencing results also revealed that alterations in several Th2 structure genes mirrored the changes observed in SerpinB2 expression, suggesting that XYP injection may regulate immune-inflammatory responses following IAV infection through targeting serpinB2. Furthermore, GO and KEGG pathway analyses implicated multiple biological functions and inflammatory signaling pathways in the immunomodulatory mechanism of XYP injection against IAV infection. The results of RNA sequencing were validated by real-time PCR of SerpinB2 and Th2 structure genes, including Ccl2, IL13ra, Tnf, Ccl3, Ccl5, IL1a, and IL1b. Subsequent experiments confirmed the binding between andrographolide and PAI-2 (SERPINB2) proteins using andrographolide-target protein chips and molecular docking. However, further validation is required to elucidate how XYP injection regulates the gene expression of SerpinB2 and the consequent alterations in its binding with PAI-2 (SERPINB2) protein.

Conclusion

In summary, our results confirm the efficacy of XYP injection in alleviating IAV infection in mice, as evidenced by reductions in mortality, weight loss, lung injury, and viral load. XYP injection demonstrated superior effects in improving inflammatory response and oxidative stress compared to dexamethasone. While XYP injection had a mild regulatory effect on the diversity of lung and fecal microbiota. It led to a notable increase in the prevalence of several potentially beneficial bacteria, particularly *Akkermansia*, *Parabacteroides goldsteinii*, *Defluviitaleaceae*, *Oscillospirales*, and *Eubacterium_coprostanoligenes_group* in the gut microbiota. Importantly, through a combination of RNA sequencing, human protein chips, and molecular docking techniques, we identified SerpinB2/PAI-2 as potential targets of XYP injection in the treatment of IAV infection and validated its regulatory effects on the expression of downstream Th2-related genes. Overall, our study provides evidence for the efficacy of XYP injection in treating IAV infection and elucidates its mechanism of immune-inflammatory regulation via targeting SerpinB2/PAI-2.

Supplementary Information

The online version contains supplementary material available at https://doi.org/10.1186/s12985-025-02636-7.

Supplementary Material 1

Supplementary Material 2

Author contributions

Tengwen Liu: Writing – original draft, Formal analysis; Shuping Li: Writing – review & editing; Xuerui Wang: Writing – original draft, Writing – review & editing, Visualization; Mingjiang Liu: Writing – original draft, Formal analysis;

Yuchen Wang: Writing – review & editing, Visualization; Jie Ying: Writing – original draft, Formal analysis; Shuwen Zhang: Writing – original draft; Formal analysis; Yan Lin: Writing – review & editing, Resources; Ning Wang: Writing – review & editing, Resources; Yungjing Bai: Writing – review & editing, Project administration; Lan Xie: Writing – review & editing; Tengfei Chen: Writing – review & editing, Conceptualization; Quansheng Feng: Writing – review & editing, Supervision; Xiaolong Xu: Writing – review & editing, Conceptualization, Supervision, Investigation. All authors contributed to the article and approved the submitted version.

Funding
This work was supported by the National Interdisciplinary Innovation Team of State Administration of Innovation Team and Talents Cultivation Program of National Administration of Traditional Chinese Medicine (ZYYCXTD-D-202201), and the High-level Key Discipline Construction Project of Traditional Chinese Medicine of National Administration of Traditional Chinese Medicine (ZYYZDXK-2023001).

Data availability
The experimental data from this study have been archived in the SAR database under accession numbers PRJNA1114924 and PRJNA1114937.

Declarations

Ethics approval and consent to participate
The animal experimentation protocols were reviewed and approved by the Experimental Animal Ethics Committee of Yangzhou University (Approval No. 202103-009).

Consent for publication
All authors approved the final manuscript.

Competing interests
The authors declare no competing interests.

Author details
[1]School of Basic Medical Sciences, Chengdu University of Traditional Chinese Medicine, Chengdu 611137, China
[2]Beijing Hospital of Traditional Chinese Medicine, Capital Medical University, Beijing 100010, China
[3]Beijing Institute of Chinese Medicine, Beijing 100010, China
[4]Beijing Key Laboratory of Innovative Research on Removing Stasis and Detoxification Theory in Infectious Diseases, Beijing 100010, China
[5]Laboratory of Clinical Medicine, Capital Medical University, Beijing 100010, China
[6]College of Veterinary Medicine, Yangzhou University, Yangzhou 225009, China
[7]Beijing University of Chinese Medicine, Beijing 100029, China
[8]Medical Systems Biology Research Center, Tsinghua University, Beijing 100084, China

Received: 9 October 2024 / Accepted: 19 January 2025
Published online: 28 January 2025

References

1 Bhattarai A, Priyadharshini A, Emerson IA. Investigating the binding affinity of andrographolide against human SARS-CoV-2 spike receptor-binding domain through docking and molecular dynamics simulations. J Biomol Struct Dyn. 2023;41(22):13438–53.
2 Bradley KC, Finsterbusch K, Schnepf D, Crotta S, Llorian M, Davidson S, Fuchs SY, Staeheli P, Wack A. Microbiota-Driven Tonic Interferon signals in lung stromal cells protect from Influenza Virus infection. Cell Rep. 2019;28(1):245–e256244.
3 Budden KF, Gellatly SL, Wood DL, Cooper MA, Morrison M, Hugenholtz P, Hansbro PM. Emerging pathogenic links between microbiota and the gut-lung axis. Nat Rev Microbiol. 2017;15(1):55–63.
4 Cani PD, Depommier C, Derrien M, Everard A, de Vos WM. Akkermansia muciniphila: paradigm for next-generation beneficial microorganisms. Nat Rev Gastroenterol Hepatol. 2022;19(10):625–37.
5 Chandramohan V, Kaphle A, Chekuri M, Gangarudraiah S, Bychapur Siddaiah G. 2015. Evaluating Andrographolide as a Potent Inhibitor of NS3-4A Protease and Its Drug-Resistant Mutants Using In Silico Approaches. Adv Virol. 2015:972067.
6 Che S, Xie X, Lin J, Liu Y, Xie J, Liu E. Andrographolide attenuates RSV-induced inflammation by suppressing apoptosis and promoting pyroptosis after respiratory syncytial virus infection in Vitro. Comb Chem High Throughput Screen. 2024;27(12):1776–87.
7 Chen Z, Wei Y, Zheng Y, Zhu H, Teng Q, Lin X, Wu F, Zhou F. 2022. SERPINB2, an Early Responsive Gene to Epigallocatechin Gallate, Inhibits Migration and Promotes Apoptosis in Esophageal Cancer Cells. Cells. 11(23).
8 Cui J, Gao J, Li Y, Fan T, Qu J, Sun Y, Liu W, Guo W, Xu Q. Andrographolide sulfate inhibited NF-kappaB activation and alleviated pneumonia induced by poly I:C in mice. J Pharmacol Sci. 2020;144(4):189–96.
9 Darnell GA, Schroder WA, Gardner J, Harrich D, Yu H, Medcalf RL, Warrilow D, Antalis TM, Sonza S, Suhrbier A. SerpinB2 is an inducible host factor involved in enhancing HIV-1 transcription and replication. J Biol Chem. 2006;281(42):31348–58.
10 Deriu E, Boxx GM, He X, Pan C, Benavidez SD, Cen L, Rozengurt N, Shi W, Cheng G. Influenza virus affects intestinal microbiota and Secondary Salmonella Infection in the gut through type I interferons. PLoS Pathog. 2016;12(5):e1005572.
11 Ding Y, Chen L, Wu W, Yang J, Yang Z, Liu S. Andrographolide inhibits influenza a virus-induced inflammation in a murine model through NF-kappaB and JAK-STAT signaling pathway. Microbes Infect. 2017;19(12):605–15.
12 Gao J, Couzens L, Burke DF, Wan H, Wilson P, Memoli MJ, Xu X, Harvey R, Wrammert J, Ahmed R et al. 2019. Antigenic drift of the Influenza A(H1N1) pdm09 Virus Neuraminidase results in reduced effectiveness of A/California/7/2009 (H1N1pdm09)-Specific antibodies. mBio. 10(2).
13 Gu X, Gao R, Li Y, Liu J, Wu Y, Xu H. Combination effect of azithromycin with TCM preparation xiyanping injection against Klebsiella pneumoniae infection in rats. Phytomedicine. 2022;104:154332.
14 Gu Z, Pei W, Shen Y, Wang L, Zhu J, Zhang Y, Fan S, Wu Q, Li L, Zhang Z. Akkermansia muciniphila and its outer protein Amuc_1100 regulates tryptophan metabolism in colitis. Food Funct. 2021;12(20):10184–95.
15 Gupta S, Mishra KP, Ganju L. Broad-spectrum antiviral properties of andrographolide. Arch Virol. 2017;162(3):611–23.
16 He W, Zhang W, Yan H, Xu H, Xie Y, Wu Q, Wang C, Dong G. Distribution and evolution of H1N1 influenza a viruses with adamantanes-resistant mutations worldwide from 1918 to 2019. J Med Virol. 2021;93(6):3473–83.
17 Lafond KE, Porter RM, Whaley MJ, Suizan Z, Ran Z, Aleem MA, Thapa B, Sar B, Proschle VS, Peng Z, et al. Global burden of influenza-associated lower respiratory tract infections and hospitalizations among adults: a systematic review and meta-analysis. PLoS Med. 2021;18(3):e1003550.
18 Lai HC, Lin TL, Chen TW, Kuo YL, Chang CJ, Wu TR, Shu CC, Tsai YH, Swift S, Lu CC. Gut microbiota modulates COPD pathogenesis: role of anti-inflammatory Parabacteroides goldsteinii lipopolysaccharide. Gut. 2022;71(2):309–21.
19 Li L, Bao J, Chang Y, Wang M, Chen B, Yan F. Gut microbiota may mediate the influence of Periodontitis on prediabetes. J Dent Res. 2021;100(12):1387–96.
20 Li Q, Li ZY, Zhang J, Guo WN, Xu XM, Sun FX, Xu H. 2019. Xiyanping Plus Azithromycin Chemotherapy in Pediatric Patients with Mycoplasma pneumoniae Pneumonia: A Systematic Review and Meta-Analysis of Efficacy and Safety. Evid Based Complement Alternat Med. 2019:2346583.
21 Liu M, Liu T, Wang X, Yu C, Qin T, Li J, Zhang M, Li Z, Cui X, Xu X, et al. Cangma Huadu granules attenuate H1N1 virus-induced severe lung injury correlated with repressed apoptosis and altered gut microbiome. Front Microbiol. 2022;13:947112.
22 Liu Q, Zhou YH, Yang ZQ. The cytokine storm of severe influenza and development of immunomodulatory therapy. Cell Mol Immunol. 2016;13(1):3–10.
23 Luo C, Zhu Y, Zhang S, Zhou J, Mao S, Tang R, Gu Y, Tan S, Lin H, Li Z, et al. Increased SERPINB2 potentiates 15LO1 expression via STAT6 signalling in epithelial cells in eosinophilic chronic rhinosinusitis with nasal polyps. Clin Exp Allergy. 2024;54(6):412–24.
24 Major LD, Partridge TS, Gardner J, Kent SJ, de Rose R, Suhrbier A, Schroder WA. Induction of SerpinB2 and Th1/Th2 modulation by SerpinB2 during lentiviral infections in vivo. PLoS ONE. 2013;8(2):e57343.
25 McAleer JP, Kolls JK. Contributions of the intestinal microbiome in lung immunity. Eur J Immunol. 2018;48(1):39–49.
26 Mikus P, Urano T, Liljestrom P, Ny T. Plasminogen-activator inhibitor type 2 (PAI-2) is a spontaneously polymerising SERPIN. Biochemical characterisation of the recombinant intracellular and extracellular forms. Eur J Biochem. 1993;218(3):1071–82.

27 Peiris JS, Poon LL, Guan Y. Emergence of a novel swine-origin influenza a virus (S-OIV) H1N1 virus in humans. J Clin Virol. 2009;45(3):169–73.
28 Piao YJ, Kim HS, Han W, Moon WK. Transcriptome analysis of SerpinB2-deficient breast tumors provides insight into deciphering SerpinB2-mediated roles in breast cancer progression. BMC Genomics. 2022;23(1):479.
29 Raja K, Prabahar A, Selvakumar S, Raja TK. In Silico Analysis to compare the effectiveness of assorted drugs prescribed for swine flu in Diverse Medicine systems. Indian J Pharm Sci. 2014;76(1):10–8.
30 Schroder WA, Le TT, Major L, Street S, Gardner J, Lambley E, Markey K, MacDonald KP, Fish RJ, Thomas R, et al. A physiological function of inflammation-associated SerpinB2 is regulation of adaptive immunity. J Immunol. 2010;184(5):2663–70.
31 Schroder WA, Major L, Suhrbier A. The role of SerpinB2 in immunity. Crit Rev Immunol. 2011;31(1):15–30.
32 Shi HY, Zhu X, Li WL, Mak JWY, Wong SH, Zhu ST, Guo SL, Chan FKL, Zhang ST, Ng SC. Modulation of gut microbiota protects against viral respiratory tract infections: a systematic review of animal and clinical studies. Eur J Nutr. 2021;60(8):4151–74.
33 Torquati L, Gajanand T, Cox ER, Willis CRG, Zaugg J, Keating SE, Coombes JS. Effects of exercise intensity on gut microbiome composition and function in people with type 2 diabetes. Eur J Sport Sci. 2023;23(4):530–41.
34 Wang G, Zhao G, Chao X, Xie L, Wang H. 2020. The characteristic of virulence, Biofilm and Antibiotic Resistance of Klebsiella pneumoniae. Int J Environ Res Public Health 17(17).
35 Wang J, Li F, Sun R, Gao X, Wei H, Li LJ, Tian Z. Bacterial colonization dampens influenza-mediated acute lung injury via induction of M2 alveolar macrophages. Nat Commun. 2013;4:2106.
36 Wu F, Guo X, Zhang J, Zhang M, Ou Z, Peng Y. Phascolarctobacterium faecium abundant colonization in human gastrointestinal tract. Exp Ther Med. 2017;14(4):3122–6.
37 Yamayoshi S, Kawaoka Y. Current and future influenza vaccines. Nat Med. 2019;25(2):212–20.
38 Ye L, Cheng L, Deng Y, Liu H, Wu X, Wang T, Chang Q, Zhang Y, Wang D, Li Z, et al. Herb-Drug Interaction between Xiyanping Injection and Lopinavir/Ritonavir, two agents used in COVID-19 pharmacotherapy. Front Pharmacol. 2021;12:773126.
39 Zhang Q, Hu J, Feng JW, Hu XT, Wang T, Gong WX, Huang K, Guo YX, Zou Z, Lin X, et al. Influenza infection elicits an expansion of gut population of endogenous Bifidobacterium animalis which protects mice against infection. Genome Biol. 2020;21(1):99.
40 Zhang X, Li PH, Wang D, Li H, Kong X, Zhang G, Zhao Y, Liu J, Wu W, Zhang Y, et al. Causal effect of gut microbiota of Defluviitaleaceae on the clinical pathway of Influenza-Subacute Thyroiditis-Hypothyroidism. Front Microbiol. 2024;15:1354989.
41 Zhang XY, Lv L, Zhou YL, Xie LD, Xu Q, Zou XF, Ding Y, Tian J, Fan JL, Fan HW, et al. Efficacy and safety of xiyanping injection in the treatment of COVID-19: a multicenter, prospective, open-label and randomized controlled trial. Phytother Res. 2021;35(8):4401–10.
42 Zhao A, Yang Z, Sun R, Grinchuk V, Netzel-Arnett S, Anglin IE, Driesbaugh KH, Notari L, Bohl JA, Madden KB, et al. SerpinB2 is critical to Th2 immunity against enteric nematode infection. J Immunol. 2013;190(11):5779–87.
43 Zhou J, Lu Y, Wu W, Feng Y. 2021. HMSC-Derived Exosome Inhibited Th2 Cell Differentiation via Regulating miR-146a-5p/SERPINB2 Pathway. J Immunol Res. 2021:6696525.

Publisher's note